## Review

# Intracellular electrochemical sensing

Kosuke Ino,*[a] Yuji Nashimoto,[a, b] Noriko Taira,[a] Javier Ramon Azcon,[c] Hitoshi Shiku*[a]

[a] Graduate School of Engineering, Tohoku University, 6-6-11 Aramaki-aza Aoba, Aoba-ku, Sendai 980-8579, Japan.
[b] Frontier Research Institute for Interdisciplinary Sciences, Tohoku University, 6-3 Aramaki-aza Aoba, Aoba-ku, Sendai 980-8578, Japan.
[c] Institute for Bioengineering of Catalonia (IBEC), The Barcelona Institute of Science and Technology, Baldiri Reixac 10-12, 08028 Barcelona Spain

Keywords: Micro/nanoelectrode; Analytical electrochemistry; Intracellular sensing; Cell analysis

*Corresponding authors: Kosuke Ino (kosuke.ino@tohoku.ac.jp) and Hitoshi Shiku (hitoshi.shiku.c3@tohoku.ac.jp)

**Abstract:**

Observing biochemical processes within living cell is imperative for biological and medical research. Fluoresce imaging is widely used for intracellular sensing of cell membranes, nuclei, lysosomes, and pH. Electrochemical assays have been proposed as an alternative to fluorescence-based assays because of excellent analytical features of electrochemical devices. Notably, thanks to the rapid progress of micro/nanotechnologies and electrochemical techniques, intracellular electrochemical sensing is making rapid progress, leading to a successful detection of intracellular components. Such insight can provide a deep understanding of cellular biological processes and, ultimately, define the human healthy and diseased states. In this review, we present an overview of recent research progress in intracellular electrochemical sensing. We focus on two main topics, electrochemical extraction of cytosolic contents from cells and intracellular electrochemical sensing *in situ*.

## 1 Introduction

Observation of biochemical intracellular processes within living cells is fundamental to a quantitative understanding of the function of biological systems. This fundamental knowledge is important in biological and medical research. To this end, fluoresce imaging is widely used to visualize nucleic acids, lysosomes, and cellular pH in real time. In the past decade, many reports on the imaging of live-cell dynamics and structure at a single-molecule level have been published [1] thanks to the rapid developments in fluorescence microscopy and fluorescence labeling techniques. For example, intracellular sensing and cell diagnostics are performed using fluorescent silica nanoparticles [2]. Fluorescent nanoparticles, including semiconductor nanoparticles (quantum dots), metal nanoparticles, and polymer nanoparticles, are also used for intracellular sensing [3].

Electrochemical approach has been proposed as an alternative to fluorescence-based assays because electrochemical devices show excellent analytical features. For example, an electrochemical method is a non-labeling and non-invasive method for the evaluation of cellular respiratory activity. Advantages of micro/nanotechnology include development of highly sensitive electrochemical assays that simultaneously incorporate many sensors, among others. Furthermore, electrochemical detection systems can be miniaturized, owing to the progress of the micro/nanotechnologies, leading to successful intracellular electrochemical sensing. The gained insight can provide a deep understanding of cellular biological processes, and can be used in several types of bio-applications, including drug testing and tissue engineering.

We have previously presented reviews on the use of microelectrode arrays in cell analysis and engineering [4], and three-dimensional (3D) cell culture using micro/nanoelectrochemical devices [5]. Further, another group reviewed electrochemical imaging of cells [6] and tissue [7]. In the current review, we focused on intracellular sensing using electrochemical devices/techniques. We divided the review into two parts, (1) electrical extraction of cytosol contents from cells and (2) intracellular electrochemical sensing *in situ*. In the former, we summarized recent studies on the harvesting of cell components using electric approaches. In the latter, we summarized *in-situ* electrochemical detection of cell-derived analytes, including endogenous enzymes, vesicles, nucleotides, reporter proteins, glucose, and $H_2O_2$.

## 2 Electrical extraction of subcellular cytosol from cells

### 2.1 Collection of subcellular cytoplasm

Several microfluidic devices have been developed for the extraction of contents of a single cell [8, 9]. Recent advances in omics technologies allow a comprehensive analysis of the genome, and gene and protein levels from such minute amounts of cytoplasm [10, 11]. However, most microfluidic approaches do not provide the spatiotemporal information on the intracellular contents because the collection methods are based on complete cell lysis. To study the dynamics of intracellular transportation or localization of cytoplasmic content [12-18], techniques for extracting subcellular cytoplasm are needed. In this section, we focused on recent electrical techniques of collecting subcellular cytoplasm (Fig. 1). Non-electrical techniques for acquiring subcellular contents are discussed in other recent papers [19, 20].

### 2.2 The use of electrical pulse for selective membrane lysis

External electric field causes a buildup of induced transmembrane voltage, resulting in pore formation in the lipid bilayer. A weak electric pulse generates temporary and limited number of pores, which can be exploited to transfer exogenous DNA to the cytoplasm (electroporation) [21]. If the electric field is too large, pore formation is too extensive and the resealing of the lipid bilayer is too slow for the cells to recover, resulting in their death and eventual disintegration. Indeed, electrical cell lysis has been used for single-cell collection [22-25].

In 2014, Shintaku et al. reported a method for the collection of cytoplasmic (cyt) RNA and nucleus, separately, from a single cell, using a microfluidic device, which utilized selective electrical lysis of the cellular membrane and isotachophoresis (ITP) (Fig. 2) [26]. First, individual cells suspended in an optimized buffer [low-mobility trailing (TE) buffer] are placed in a microfluidic channel filled with another ITP buffer [high-mobility leading electrolyte (LE) buffer]. Then, a bipolar voltage pulse (3000 V, 100 ms) is applied (Figs. 2A and 2B). The calculated potentials across the cell membrane are around 3 V. This is high in comparison with the typical breakdown voltage of the cell membrane (1 V), while the nuclear membranes are kept intact. Immediately after the lysis of the cellular membrane, a direct current (DC) electric field is applied in the same channel to initiate ITP, to focus RNA at an ITP interface between TE and LE [27]. During the ITP, two (fluorescent) nucleic acid regions are apparent: the first is the concentrated total cytoplasmic RNA and the second, with an ellipsoidal shape, is the nucleus. Although total RNA and the nuclei both migrate toward the same outlet where the negative electrode is inserted, the authors successfully separated the RNA from the nucleus because of the difference of their migration velocities (Fig. 2C). Using on-chip quantification of fluorescently labeled nucleic acids, the authors demonstrated the

heterogeneity of nucleic acid amounts depending on the cell cycle. A year later, the same group demonstrated the collection of the separated RNA and the nucleus from the microfluidic device, and utilized the collected material for sequence-specific analysis (qPCR) [28].

More recently, Shintaku and colleagues improved the design of the device for a highly automated nuclear (nucRNA) and cytRNA collection, and conducted comprehensive RNA sequencing, termed single-cell integrated nucRNA and cytRNA-sequencing (SINC-seq) [29]. They analyzed 93 single cells (generating 186 RNA-seq libraries with RNA-seq) and, after careful quality control, they acquired 84 single-cell datasets. By comparing the *in-silico* single-cell data (cytRNA-seq + nucRNA-seq) with those of traditional single-cell RNA-seq, they demonstrated excellent correspondence between the average gene expression profiles obtained via the two approaches, indicating the reliability of SINC-seq for subcellular analyses. By using SINC-seq, the authors also showed three different correlations of cytRNA with nucRNA; 1) highly correlated expression in cell-cycle-related genes, 2) the distorted correlation via nuclear-retained introns, 3) the correlation dynamics along the cell differentiation [29].

### 2.3 Nanostraw-electroporation system

Melosh and colleagues developed an alternative method for the analysis of subcellular contents of living cells using a nanostraw-electroporation system, termed nanostraw extraction (NEX) [30]. NEX setup is composed of two-layer compartments separated vertically by a polymer membrane with an array of hollow nanostraws. The bottom of the device is made of indium tin oxide (ITO) and a Pt electrode is inserted into the top layer (Figs. 3A and 3B).

The nanostraws are fabricated from commercially available track-etched polycarbonate membranes [31]. Briefly, a thin alumina coating (10–30-nm thick) is deposited on a track-etched membrane ($1 \times 10^8$ pores/cm$^2$) by atomic layer deposition (ALD); this will become the nanostraw wall. Reactive ion etching (RIE) and oxygen plasma are used to remove the aluminum and polycarbonate, respectively, and then a nanostraw array is formed. Nanostraws with a diameter smaller than 100 nm directly penetrate the cellular membrane, while larger nanostraws do not [31, 32]. For NEX, the authors selected the 150-nm diameter nanostraws to prevent continuous leakage of cytosol from the target cells (Fig. 3C).

In another study, to sample the cellular contents by NEX, 10–35 V square electric pulses (200 μs, 20 Hz) were applied between the ITO and Pt electrode for 20–60

s [33]. Small pores in the cellular membranes temporarily appear at the nanostraw-cellular membrane interface after an electric pulse, and the intracellular contents move to the bottom layer filled with PBS. Although the extraction process mainly relies on free diffusion of the cellular contents, the positive potential of the ITO electrode facilitates the movement of the negatively charged contents to the bottom layer from the cytoplasm. After the electrical pulse, the cellular membrane recovers within a few minutes, similarly to a conventional electroporation system [34, 35]. The connection between the cytoplasm and the bottom layer disappeared at least as early as 10 min after the electrical pulse [33]. Using the transient pore opening as a valve, they were able to repeatedly collect the cytoplasm, with cell viability of >95%. The extracted proteins were then concentrated by ITP and their amounts determined by fluorescent intensity or enzymatic assay (ELISA). Quantitative analysis revealed that NEX extracted 7–8% of the cytoplasm and that approximately 70% of the extracted proteins could be detected using the system. NEX was also used to monitor the status of induced pluripotent stem cells (iPSCs) for 5 d. The up-regulation of HSP27 in iPSCs exposed to a heat shock was successfully detected by continuous NEX monitoring. In addition, the authors performed a comprehensive gene expression analysis of the extracted cytoplasmic material. Although the sensitivity of NEX did not allow detection of transcripts from a single cell, 41 mRNA molecules were accurately quantified from samples of 15–20 cells. The study [30] was the first to demonstrate time-resolved, longitudinal extraction of contents from the same cells in a highly quantitative manner.

### 2.4 Dielectrophoretic nanotweezers (DENT)

Atomic force microscopy (AFM) had been used for the collection of intracellular contents for 15 years [36-39]. An AFM probe is inserted into the cytoplasm, and then the proteins and transcripts are adsorbed onto the surface of the probe. Although AFM can be used to collect cellular contents in a minimally invasive manner and from any area of the target cell, with nanoscale accuracy, the targets were initially limited to highly expressed molecules because the collection method mainly relied on a nonspecific adsorption to the probe. To address that, Wickramasinghe and colleagues reported the design of dielectrophoretic nanotweezers (DENT) that can be used to extract mRNA present at very low copy numbers (100 copies/cell) (Fig. 4) [40, 41].

The DENT fabrication process starts with commercially available conical highly doped silicon AFM probes. First, a 20-nm thick layer of $SiO_2$ is deposited on the AFM probe, insulating the entire AFM probe. Then, Ti/Pt [41, 42] or Cr/Au [40, 43] layer is deposited by evaporation onto the $SiO_2$ layer to serve as the electrode. Finally, the

probe tip is polished until the inner silicon core is exposed (Fig. 4A). When an alternating current (AC) field is applied between the silicon core and the outer electrode, non-uniform electric field is created at the tip of the probe, and dielectrophoretic (DEP) force is generated (Fig. 4B). mRNA molecules preferentially move toward the probe-end because of the strong positive DEP force generated at the probe-end. The extracted mRNA molecules can then be released from the DENT probe into a PCR tube and quantified by qPCR (Fig. 4C). Since DEP can be used to manipulate single cells [44, 45], DEP techniques could be developed for both, cell manipulation and cytosolic extraction, in the future.

In their early work, Wickramasinghe and colleagues have simply shown that the DENT probe can be used to extract more mRNA molecules than a conventional AFM probe [41, 42]. Recently, the authors optimized DEP conditions for mRNA extraction: they showed than an applied AC field of 1.5 peak-to-peak voltage (Vp-p, 10 MHz) does not affect the viability of the target cell and that low-abundance mRNA molecules (hypoxanthine phosphoribosyltransferase, *HPRT*, 100 copies/cell) can be detected using the system. Lower voltage reduced the number of molecules attached to the probe, while voltage above 1.5 Vp-p affected protein expression in the target cell, probably because too many mRNA molecules were extracted [40]. In this study, DENT was integrated with a microfluidic system for high-throughput analysis. The microfluidic device contained an array of 100 single-cell traps and could be used to capture single cells from a suspension within 20 s. The top layer of the array was made of ultra-thin PDMS membrane (1-μm thick) so that the DENT probe would penetrate the PDMS membrane and access the target single cells in the microfluidic device. The authors successfully used the device for multiple gene expression analysis of two types of target cells mimicking the normal blood sample [40].

### 2.5 Integration with scanning ion-conductance microscopy (SICM)

SICM is a nanopipette-based technique that enables imaging of the topography of a target sample [46-48]. In a typical SICM setup, a single-barrel nanopipette is filled with an electrolyte solution (PBS, etc.) and a reference electrode (Ag/AgCl) is inserted into the nanopipette. Another reference electrode is placed in bulk solution and a potential bias is applied between the two reference electrodes to generate an ionic current through the tip of the nanopipette. In SICM, the magnitude of the ion current at the tip is used as a feedback signal to control the nanopipette-sample distance. When the nanopipette approaches the sample, the ion current decreases because the resistance between the nanopipette and sample increases. Because SICM does not

involve physical contact with the target cells, the nanopipette approach can be used to analyze a sample under physiological condition [47, 49-53] and in a non-invasive manner [50, 54-57].

In 2014, Pourmand and colleagues integrated SICM with an electrochemical attosyringe [58], which enabled the extraction of RNA and organelles from a single living cell [59]. A nanopipette filled with an organic electrolyte solution [10 mM tetrahexylammonium tetrakis-(4-chlorophenyl)borate (THATPBCl) in 1,2-dichloroethane (DCE)] was used as a SICM probe in the system. When the nanopipette is immersed in an aqueous solution, an oil-water interface is formed at the tip of the nanopipette. The oil-water interface can be controlled by a potential applied to the reference electrode in the nanopipette (Ag/AgTPBCl). When a positive potential is applied, the outer aqueous solution cannot enter the nanopipette (Fig. 5A, a-i). When a negative potential is applied, the interface moves up, and the aqueous solution can be collected into the pipette (Fig. 5A, a-ii). When the potential moves back to negative, the collected solution is released from the pipette (Fig. 5A, a-iii). Although the detailed mechanism of how the electrochemical attosyringe works has not been elucidated, it has been proposed that electrowetting, electrophoresis, and electroosmosis are the driving forces of the interface movement [58-60].

The Pourmand group collected the cytosol as follows (Fig. 5B) [59]. First, by monitoring the ion current at the tip, the nanopipette approached within 1 μm of the target single cell. During the approach, the potential in the nanopipette was kept positive to prevent the aqueous solution from entering the pipette. Then, the nanopipette was moved down from the position of approach, piercing the cellular membrane, and the tip entered the cytoplasm. After the penetration, the potential inside the nanopipette was changed to negative so that the oil-water interface moved up and the cytoplasm could be collected. The authors demonstrated that the collected mRNA and organelles (mitochondria) could be used for qPCR, and DNA [59] and RNA [61] sequencing. The analysis revealed the heterogeneities of mRNA and organelles in the targeted single cells.

In another study, Shiku and colleagues reported lamination of three aqueous phases that contained nucleic acid labeled using different tags [60]. Each aqueous phase was separated by an organic phase. The authors named this system the “mille-feuille” probe, and showed that it could be used for sequential collection of different samples.

Two years later, Shiku and colleagues combined the nanopipette with a high-resolution mapping function (Fig. 5C) [62]. To stably control the oil-water interface in the nanopipette, the concentration of the electrolyte in organic solution should be

below 10 mM [58]; however, such low concentration of electrolyte cannot generate sufficient ion current to regulate the pipette position for high-resolution topography. The authors employed a double-barrel SICM, filling each barrel with either an aqueous or organic electrolyte solution. The aqueous solution barrel was used for topographical mapping and the organic solution barrel was used as the electrochemical syringe. The authors confirmed that the electrochemical syringe was operational in the double-barrel nanopipette and that the aqueous barrel allowed acquisition of high-resolution topography images (Fig. 5C). Utilizing the system, they successfully collected the cytoplasm at two different loci within a single cell. They then used qPCR to compare gene expression in the samples. The analysis revealed that the expression of the *Actb* gene was different depending on location within the target single cell. The collection methods using SICM and AFM are highly promising because these methods allow spatiotemporal analysis of the target cytoplasm.

## 3 Electrochemical intracellular sensing *in situ*

In this section, we provide an overview of intracellular electrochemical sensing *in situ* approaches that adapted amperometry and potentiometry. We discussed the following: (1) a double-mediator system for monitoring intracellular enzymes; (2) monitoring vesicles containing redox compounds and secreted chemicals; (3) gene analysis within cells; (4) detection of intracellular glucose; (5) detection of intracellular electrochemiluminescence (ECL); and (6) electrochemical impedance spectroscopy (EIS).

### 3.1 Intracellular redox sensing using a double-mediator system

Several types of redox mediators are used to detect redox enzymes within cells in a number of approaches [63] because these mediators can shuttle electrons between the electrode and the enzymes. One such approach is a double-mediator system involving menadione. Menadione is widely used because it is a hydrophobic redox mediator the can pass through the cell membrane.

In one system, menadione shuttles the electrons from intracellular enzymes to extracellular ferrocyanide, a compound whose permeability of the cell membrane is low. This particular system was used to detect NAD(P)H-oxidizing enzymes (NOEs) of *Saccharomyces cerevisiae* strain Y190 (Fig. 6) [64]. In addition to single yeast cells, the system was used to monitor the activity of intracellular quinone oxidoreductase of single cancer cell line (HeLa) cells [65].

Another double-mediator system, based on menadione and osmium redox polymer (PVI-Os), was also reported [66]. Conversely, instead of menadione,

2,6-dichlorophenolindophenol (DCPIP) can also be used [67]. In the latter study, the dual-mediator system was employed to assess the relationship between the redox activities and the fermentation efficiency of yeast. As yet another possible application, a whole cell-based biosensor with double mediators was used to monitor the acute biotoxicity of wastewater in another study [68]. This clearly demonstrates the utility of the double-mediator system for the detection of intracellular redox enzymes.

### 3.2 Electrochemical detection of secreted vesicles, chemicals, and proteins

For a conventional electrochemical detection, micro/nanoelectrode is placed outside cells to monitor oxidation currents of secreted vesicles containing dopamine from neuron and neuron-like cells [69]. By contrast, flame-etched carbon-fiber nanotip electrodes have been adapted to monitor these vesicles within cells, enabling the detection of the intracellular catecholamine content of individual nanoscale vesicles in PC12 cells (Fig. 7) [70]. The nanotip electrode can be inserted in the cells without substantial damage of the membrane.

Further, electrode arrays are used for imaging and mapping of dopamine released from cells [71, 72]. Recently, a new electrochemical imaging approach based on electrode arrays, designated “electrochemicolor imaging” [72, 73], was developed for simultaneous detection of multiple analytes, such as dopamine and dissolved oxygen. By using the imaging system, dopamine release and respiratory activity of neuron-like cells were successfully imaged in real time (Fig. 8). This electrochemical imaging system is likely to reveal the relationship between these cellular activities in the future.

Electrochemical detection is also useful for the analysis of vesicles outwith and within cells. In the future, other vesicles, including exosomes, could be monitored as they attract a lot of attention [74]. Already, some biosensors for exosomes based on aptamers [75] and for exosomal microRNAs [76] have been reported.

As mentioned above, SICM can be used to analyze cell topology. E.g., the levels of von Willebrand factor, a secretory protein, were determined in living cells by using this technique [77]. SICM is an attractive tool for cell topography analysis [50, 55, 78, 79] because of its low invasiveness and no requirement of labeling. SICM can also be combined with other electrochemical techniques, such as SECM, for chemical mapping [54, 80, 81]. Therefore, it is very likely that this technique will be widely utilized for intracellular analyses in near future.

Finally, cell activity can be electrochemically detected by using marker proteins, such as endogenous alkaline phosphatase (ALP). For example, cell differentiation of embryonic stem cells [72, 82-85] and early-stage bone differentiation [73] have been

electrochemically detected. Several types of integrated electrochemical devices have been developed for bioanalysis including cell analysis and they are discussed in detail elsewhere [4, 5]. The electrochemical approach can be utilized for organ transplantation and quality assurance of stem cells.

### 3.3 Electrochemical gene analysis

Another application of electrochemical intracellular sensing *in situ* are electrochemical reporter gene assays for the detection of gene expression within cells [86-90]. In the assays, the activity of a reporter protein, such as secreted alkaline phosphatase (SEAP) or *β*-galactosidase (*β*-gal), is monitored electrochemically. For example, an electrode can be used to detect *β*-gal inside cells as a reporter, with its gene expressed from a promoter of choice, or a combination of genetic elements, in response to various molecular cues [90]. As shown in Fig. 9, the enzymatic substrate 4-aminophenyl *β*-D-galactopyranoside (PAPG) is cleaved by *β*-gal into *p*-aminophenol (PAP), which is then oxidized at an electrode outside the cell. PAP oxidation current indicates gene expression and the activity of cell signaling pathways. Further, electrochemical reporter gene assays with microfluidics can be utilized for whole-cell electrochemical sensing to analyze hormone-active chemicals [86].

To electrochemically detect target DNA and RNA molecules, electrodes with attached DNA probes are widely used [91]. After hybridization of the targets and probes, electrochemical signal is detected using an electrochemical indicator (labeled enzymes or redox compounds). For example, in one study, mRNA was detected in living cells using an electrode with attached DNA [92]. In that study, a probe interacted with mRNA inside a living cell, and the electrode was used to monitor the changes of electron transfer efficiency between ferrocene (Fc) modified by the attached DNA and the electrode surface (Fig. 10).

To conclude, gene expression can indeed be determined using electrochemical approaches. For high-throughput analysis, electrode arrays and capillary arrays may be used, so that local gene expression within cells may be studied.

### 3.4 Detection of glucose within cells

Since glucose is a key compound for cell activity, its detection is of interest. As an example of an approach for intracellular glucose sensing, nanopipette was functionalized as a glucose nanosensor by covalently immobilizing glucose oxidase (GOx) on the tip. The interaction of glucose with GOx resulted in a catalytic oxidation of glucose to gluconic acid, which was observed as a change in impedance associated with a

drop in medium pH at the nanopipette tip (Fig. 11A) [93].

Detection of intracellular glucose using a functionalized ZnO-nanorod–based selective electrochemical sensor was also reported [94]. For the detection, potential difference between the electrode and Ag/AgCl was monitored.

As another example, a nanometer-sized capillary with a ring electrode was used to detect intracellular glucose (Fig. 11B) [95]. There, a GOx solution filled the tip capillary, and the capillary was inserted into cells. It was then pumped into the cells, and the reaction by-product was detected using the ring electrode [95].

### 3.5 ECL-based detection of molecules within cells

In addition to potentiometric and amperometric sensors discussed above, ECL is also widely used for intracellular sensing. For example, in one study, intracellular $H_2O_2$ was visualized using a comprehensive Au-luminol microelectrode and ECL (Fig. 12A) [96]. For the detection, a capillary was filled with a mixture of chitosan and luminol; then, a thin layer of gold was sputtered onto the capillary. Finally, luminescence was generated at the tip in the presence of $H_2O_2$.

ECL technology was also used to detect intracellular telomerase activity in HL-60 cancer cells [97]. After polyluminol-Pt NPs was electrodeposited on an electrode, an aptamer modified to recognize the HL-60 cancer cells was used, and ECL signals induced (Fig. 12B). Luminol ECL was also applied in the analysis of intracellular molecules, such as glucose, in single cells [98]. In that case, the cells were simultaneously treated with luminol, Triton X-100, and GOx. Disruption of the cellular membrane released intracellular glucose into microwells, resulting in ECL.

In another study, active membrane cholesterol in a single living cell was imaged via detection of $H_2O_2$ generated by a reaction between cholesterol and cholesterol oxidase [99]. Cholesterol in the plasma membrane of single cells can also be detected by using a microcapillary electrode filled with a mixture of cholesterol oxidase and Triton X-100 [100].

Membrane cholesterol and intracellular cholesterol can be analyzed on a single-cell level in a two-step setup [101]. The cells are first placed on a microarray modified by an inclusion of g-$C_3N_4$ nanosheet. They are then exposed to cholesterol oxidase to generate $H_2O_2$, resulting in chemiluminescence of membrane cholesterol. The cells are treated with Triton X-100, cholesterol esterase, and cholesterol oxidase to generate $H_2O_2$. This enables the detection of luminescence associated with intracellular cholesterol [101].

When a cell is analyzed by ECL, steric hindrance and cell insulation become

problematic. As a solution to this problem, direct ECL imaging of a single cell using chitosan and fluoride-doped tin oxide conductive glass modified with nano-$TiO_2$ (FTO/$TiO_2$/CS) was developed [102]. A cell immobilized on chitosan and FTO/$TiO_2$/CS was first stimulated by *N*-formylmethionyl-leucyl-phenylalanine; $H_2O_2$ was consequently released by individual cells, resulting in ECL of luminol (Fig. 12C).

Since ECL is a highly sensitive detection technique that combines the advantages of both, electrochemical and chemiluminescence methods, it will likely be used for intracellular analyses in the future.

### 3.6 Intracellular EIS analysis

EIS is a sensitive technique based on monitoring the electrical response of a studied system after application of a periodic small-amplitude AC signal over a large range of frequencies. Analysis of the response of the system provides information concerning the electric properties of the dynamics of bound or mobile charges in the bulk or interfacial regions of any type of material (solid or liquid), at the sensor-sample interface, and the reactions occurring thereat [103, 104]. In recent years, EIS has shown widespread applicability in biotechnology, tissue engineering, cell characterization, disease diagnosis, and cell culture monitoring.

Until now, the use of impedance in biomaterial applications has been limited by a number of factors, such as the inability to accurately measure the extremely low currents involved, poor scalability, lack of specificity, and the need for safe working when performing experiments with living tissue. However, its capabilities for probing interfacial properties of biomolecular films at the electrode surface are superior to virtually all other electrochemical techniques [105]. Some examples of studies involving cell culture monitoring, and real-time monitoring of changes in endothelial monolayers and cell spreading may be found [106, 107], but the detail of intracellular information that can be obtained from cells remains quite limited. EIS can be developed to address these limitations. For instance, using nanoscale intracellular electrodes with integrated complementary metal-oxide-semiconductor (CMOS) circuits, Abbot et al. were able to measure the intracellular membrane potentials from hundreds of connected *in vitro* neonatal rat ventricular cardiomyocytes [108]. As another example, Li et al. pioneered the use of ultrasensitive EIS for the quantification of both external (tetraspanin) and internal (syntenin) exosome-specific markers [109].

## 4 Perspectives and conclusions

In this review, we summarized recent studies on the intracellular

electrochemical sensing. We discussed mainly two topics, electrical extraction of subcellular cytosol from cells and intracellular sensing in *situ*. Since small amounts of cell components can be extracted using electrochemical devices, and these components can then be analyzed using several types of methods, including PCR, the described devices are more useful for intracellular sensing than intracellular sensing *in situ*. By contrast, electrochemical sensing *in situ* has been widely used because it allows real-time monitoring of target analytes.

Thanks to the rapid progress of micro/nanotechnology, cells can be electrochemically analyzed without cell damage. Although probe-based devices are widely used for intracellular electrochemical sensing, electrode arrays and microfluidic devices may be used for high-throughput analysis and rapid electrochemical imaging in real time. Since 3D cell cultures are attracting great attention, intracellular sensing in such 3D-cultured cells and tissues will likely be widely monitored using electrochemical approaches in the future. Reviews of electrochemical imaging of 3D cell cultures and tissues have been recently published [5, 7]. Promisingly, electrochemical approaches can be combined with organ-on-a-chip systems, which mimic organs in microfluidics [110]. Since the vascular system is important for organs, vascular constructions have been already incorporated into organs-on-a-chip [111]. Consequently, the function of the vascular system can be electrochemically evaluated in such organs-on-a-chip, e.g., as shown by monitoring of nitric oxide (NO) release by endothelial cells [112, 113]. Further, since some intracellular phenomena derive from electrochemical reactions, electrochemistry might be able to comprehensively describe the intracellular environment in the future [114].

Although this review focused on intracellular sensing using electrodes, electrochemical reactions can also be applied to biofabrication. For example, an electrochemical device can be utilized to electrodeposit hydrogels. Cells have been successfully cultured in such hydrogels [115-117]. By combining biofabrication with electrode arrays into a sensing system, a novel cell culture platform with sensors may be constructed. In addition, the platform can be applied to electrochemical organs-on-a-chip.

## Acknowledgements

This work was supported by a Grant-in-Aid for Scientific Research (A) (No. 16H02280), a Grant-in-Aid for Scientific Research (B) (Nos. 15H035420, 18H01840 and 18H01999), a Grant-in-Aid for Young Scientists (A) (No. 15H05415), and a Grant-in-Aid for Young Scientists (B) (16K16386) from the Japan Society for the Promotion of Science

(JSPS). This work was also supported by Research Grant from the Nakatomi Foundation.

## References


[1] Z. Liu, L.D. Lavis, E. Betzig, *Mol. Cell* **2015**, *58*, 644-659.

[2] A. Schulz, C. McDonagh, *Soft Matter* **2012**, *8*, 2579-2585.

[3] M.J. Ruedas-Rama, J.D. Walters, A. Orte, E.A.H. Hall, *Anal. Chim. Acta* **2012**, *751*, 1-23.

[4] K. Ino, H. Shiku, T. Matsue, *Curr. Opin. Electrochem.* **2017**, *5*, 146-151.

[5] K. Ino, M. Sen, H. Shiku, T. Matsue, *Analyst* **2017**, *142*, 4343-4354.

[6] R.A. Lazenby, R.J. White, *Chemosensors* **2018**, *6*, 24.

[7] T.E. Lin, S. Rapino, H. Giraulta, A. Lesch, *Chem. Sci.* **2018**, *9*, 4546-4554.

[8] S.J. Hosic, S.K. Murthy, A.N. Koppes, *Anal. Chem.* **2016**, *88*, 354-380.

[9] T.W. Murphy, Q. Zhang, L.B. Naler, S. Ma, C. Lu, *Analyst* **2018**, *143*, 60-80.

[10] Y. Hou, H. Guo, C. Cao, X. Li, B. Hu, P. Zhu, X. Wu, L. Wen, F. Tang, Y. Huang, J. Peng, *Cell Res.* **2016**, *26*, 304-319.

[11] D. Wang, S. Bodovitz, *Trends Biotechnol.* **2010**, *28*, 281-290.

[12] L. Zhang, A. Vertes, *Angew. Chem. Int. Ed.* **2018**, *57*, 4466-4477.

[13] P.J. Thul, L. Akesson, M. Wiking, D. Mahdessian, A. Geladaki, H. Ait Blal, T. Alm, A. Asplund, L. Bjork, L.M. Breckels, A. Backstrom, F. Danielsson, L. Fagerberg, J. Fall, L. Gatto, C. Gnann, S. Hober, M. Hjelmare, F. Johansson, S. Lee, C. Lindskog, J. Mulder, C.M. Mulvey, P. Nilsson, P. Oksvold, J. Rockberg, R. Schutten, J.M. Schwenk, A. Sivertsson, E. Sjostedt, M. Skogs, C. Stadler, D.P. Sullivan, H. Tegel, C. Winsnes, C. Zhang, M. Zwahlen, A. Mardinoglu, F. Ponten, K. von Feilitzen, K.S. Lilley, M. Uhlen, E. Lundberg, *Science* **2017**, *356*, eaal3321.

[14] O. Guillaume-Gentil, T. Rey, P. Kiefer, A.J. Ibanez, R. Steinhoff, R. Bronnimann, L. Dorwling-Carter, T. Zambelli, R. Zenobi, J.A. Vorholt, *Anal. Chem.* **2017**, *89*, 5017-5023.

[15] L. Xing, G.J. Bassell, *Traffic* **2013**, *14*, 2-14.

[16] C. Medioni, K. Mowry, F. Besse, *Development* **2012**, *139*, 3263-3276.

[17] K.C. Martin, A. Ephrussi, *Cell* **2009**, *136*, 719-730.

[18] D. St Johnston, *Nat. Rev. Mol. Cell Biol.* **2005**, *6*, 363-375.

[19] P. Actis, *Small Methods* **2018**, *2*, 1700300.

[20] S.G. Higgins, M.M. Stevens, *Science* **2017**, *356*, 379-380.

[21] M.L. Yarmush, A. Golberg, G. Sersa, T. Kotnik, D. Miklavcic, *Annu. Rev. Biomed. Eng.* **2014**, *16*, 295-320.

[22] F.T. Han, Y. Wang, C.E. Sims, M. Bachman, R.S. Chang, G.P. Li, N.L. Allbritton, *Anal. Chem.* **2003**, *75*, 3688-3696.

[23] Y. Nashimoto, Y. Takahashi, T. Yamakawa, Y.S. Torisawa, T. Yasukawa, T. Ito-Sasaki, M. Yokoo, H. Abe, H. Shiku, H. Kambara, T. Matsue, *Anal. Chem.* **2007**, *79*,

6823-6830.
[24] Y. Nashimoto, Y. Takahashi, R. Takano, K. Miyashita, S. Yamada, K. Ino, H. Shiku, T. Matsue, *Anal. Bioanal. Chem.* **2014**, *406*, 275-282.
[25] H. Ito, Y. Nashimoto, Y. Zhou, Y. Takahashi, K. Ino, H. Shiku, T. Matsue, *Anal. Chem.* **2016**, *88*, 610-613.
[26] H. Shintaku, H. Nishikii, L.A. Marshall, H. Kotera, J.G. Santiago, *Anal. Chem.* **2014**, *86*, 1953-1957.
[27] R.B. Schoch, M. Ronaghi, J.G. Santiago, *Lab Chip* **2009**, *9*, 2145-2152.
[28] K. Kuriyama, H. Shintaku, J.G. Santiago, *Electrophoresis* **2015**, *36*, 1658-1662.
[29] M.N. Abdelmoez, K. Iida, Y. Oguchi, H. Nishikii, R. Yokokawa, H. Kotera, S. Uemura, J.G. Santiago, H. Shintaku, *Genome Biol.* **2018**, *19*, 66.
[30] Y. Cao, M. Hjort, H. Chen, F. Birey, S.A. Leal-Ortiz, C.M. Han, J.G. Santiago, S.P. Pasca, J.C. Wu, N.A. Melosh, *Proc. Natl. Acad. Sci. U. S. A.* **2017**, *114*, E1866-E1874.
[31] J.J. VanDersarl, A.M. Xu, N.A. Melosh, *Nano Lett.* **2012**, *12*, 3881-3886.
[32] A.M. Xu, A. Aalipour, S. Leal-Ortiz, A.H. Mekhdjian, X. Xie, A.R. Dunn, C.C. Garner, N.A. Melosh, *Nat. Commun.* **2014**, *5*, 3613.
[33] X. Xie, A.M. Xu, S. Leal-Ortiz, Y. Cao, C.C. Garner, N.A. Melosh, *ACS Nano* **2013**, *7*, 4351-4358.
[34] Z.C. Lin, C. Xie, Y. Osakada, Y. Cui, B. Cui, *Nat. Commun.* **2014**, *5*, 3206.
[35] D.C. Chang, T.S. Reese, *Biophys. J.* **1990**, *58*, 1-12.
[36] S.-W. Han, H.-K. Shin, S.-H. Ryu, C. Nakamura, *J. Nanosci. Nanotechnol.* **2016**, *16*, 8674-8677.
[37] T. Kihara, N. Yoshida, T. Kitagawa, C. Nakamura, N. Nakamura, J. Miyake, *Biosens. Bioelectron.* **2010**, *26*, 1449-1454.
[38] H. Uehara, T. Osada, A. Ikai, *Ultramicroscopy* **2004**, *100*, 197-201.
[39] T. Osada, H. Uehara, H. Kim, A. Ikai, *J. Nanobiotechnol.* **2003**, *1*, 2.
[40] X. Li, Y. Tao, D.H. Lee, H.K. Wickramasinghe, A.P. Lee, *Lab Chip* **2017**, *17*, 1635-1644.
[41] D. Nawarathna, R. Chang, E. Nelson, H.K. Wickramasinghe, *Anal. Biochem.* **2011**, *408*, 342-344.
[42] D. Nawarathna, T. Turan, H.K. Wickramasinghe, *Appl. Phys. Lett.* **2009**, *95*, 83117.
[43] Y. Tao, H.K. Wickramasinghe, *Appl. Phys. Lett.* **2017**, *110*, 073701.
[44] T. Matsue, N. Matsumoto, S. Koike, I. Uchida, *Biochim. Biophys. Acta* **1993**, *1157*, 332-335.
[45] S. Ogata, T. Yasukawa, T. Matsue, *Bioelectrochemistry* **2001**, *54*, 33-37.
[46] J. Zhuang, R. Guo, F. Li, D. Yu, *Meas. Sci. Technol.* **2016**, *27*, 085402.

[47] Y.E. Korchev, C.L. Bashford, M. Milovanovic, I. Vodyanoy, M.J. Lab, *Biophys. J.* **1997**, *73*, 653-658.
[48] P.K. Hansma, B. Drake, O. Marti, S.A. Gould, C.B. Prater, *Science* **1989**, *243*, 641-643.
[49] S. Zhang, S.J. Cho, K. Busuttil, C. Wang, F. Besenbacher, M. Dong, *Nanoscale* **2012**, *4*, 3105-3110.
[50] Y. Takahashi, Y. Murakami, K. Nagamine, H. Shiku, S. Aoyagi, T. Yasukawa, M. Kanzaki, T. Matsue, *Phys. Chem. Chem. Phys.* **2010**, *12*, 10012-10017.
[51] J. Gorelik, L.Q. Yang, Y. Zhang, M. Lab, Y. Korchev, S.E. Harding, *Cardiovasc. Res.* **2006**, *72*, 422-429.
[52] J. Gorelik, A.I. Shevchuk, G.I. Frolenkov, I.A. Diakonov, M.J. Lab, C.J. Kros, G.P. Richardson, I. Vodyanoy, C.R. Edwards, D. Klenerman, Y.E. Korchev, *Proc. Natl. Acad. Sci. U. S. A.* **2003**, *100*, 5819-5822.
[53] Y.E. Korchev, J. Gorelik, M.J. Lab, E.V. Sviderskaya, C.L. Johnston, C.R. Coombes, I. Vodyanoy, C.R. Edwards, *Biophys. J.* **2000**, *78*, 451-457.
[54] Y. Takahashi, A.I. Shevchuk, P. Novak, Y. Murakami, H. Shiku, Y.E. Korchev, T. Matsue, *J. Am. Chem. Soc.* **2010**, *132*, 10118-10126.
[55] Y. Zhou, M. Saito, T. Miyamoto, P. Novak, A.I. Shevchuk, Y.E. Korchev, T. Fukuma, Y. Takahashi, *Anal. Chem.* **2018**, *90*, 2891-2895.
[56] J. Rheinlaender, N.A. Geisse, R. Proksch, T.E. Schaffer, *Langmuir* **2011**, *27*, 697-704.
[57] Y. Takahashi, A.I. Shevchuk, P. Novak, Y.J. Zhang, N. Ebejer, J.V. Macpherson, P.R. Unwin, A.J. Pollard, D. Roy, C.A. Clifford, H. Shiku, T. Matsue, D. Klenerman, Y.E. Korchev, *Angew. Chem. Int. Ed.* **2011**, *50*, 9638-9642.
[58] F.O. Laforge, J. Carpino, S.A. Rotenberg, M.V. Mirkin, *Proc. Natl. Acad. Sci. U. S. A.* **2007**, *104*, 11895-11900.
[59] P. Actis, M.M. Maalouf, H.J. Kim, A. Lohith, B. Vilozny, R.A. Seger, N. Pourmand, *ACS Nano* **2014**, *8*, 546-553.
[60] H. Ito, M. Tanaka, Y. Zhou, Y. Nashimoto, Y. Takahashi, K. Ino, T. Matsue, H. Shiku, *Anal. Bioanal. Chem.* **2017**, *409*, 961-969.
[61] E.N. Toth, A. Lohith, M. Mondal, J. Guo, A. Fukamizu, N. Pourmand, *J. Biol. Chem.* **2018**, *293*, 4940-4951.
[62] Y. Nashimoto, Y. Takahashi, Y. Zhou, H. Ito, H. Ida, K. Ino, T. Matsue, H. Shiku, *ACS Nano* **2016**, *10*, 6915-6922.
[63] F.J. Rawson, A.J. Downard, K.H. Baronian, *Sci. Rep.* **2014**, *4*, 5216.
[64] K. Nagamine, Y. Takahashi, K. Ino, H. Shiku, T. Matsue, *Electroanalysis* **2011**, *23*,

576 1168-1174.
577 [65] Y. Matsumae, Y. Takahashi, K. Ino, H. Shiku, T. Matsue, *Anal. Chim. Acta* **2014**,
578 *842*, 20-26.
579 [66] A. Heiskanen, V. Coman, N. Kostesha, D. Sabourin, N. Haslett, K. Baronian, L.
580 Gorton, M. Dufva, J. Emneus, *Anal. Bioanal. Chem.* **2013**, *405*, 3847-3858.
581 [67] J. Zhao, Z. Wang, C. Fu, M. Wang, Q. He, *Electroanalysis* **2008**, *20*, 1587-1592.
582 [68] G.Y. Gao, D.Y. Fang, Y. Yu, L.Z. Wu, Y. Wang, J.F. Zhi, *Talanta* **2017**, *167*, 208-216.
583 [69] N.T.N. Phan, X. Li, A.G. Ewing, *Nat. Rev. Chem.* **2017**, *1*, 0048.
584 [70] X. Li, S. Majdi, J. Dunevall, H. Fathali, A.G. Ewing, *Angew. Chem. Int. Ed.* **2015**, *54*,
585 11978-11982.
586 [71] H. Abe, K. Ino, C.Z. Li, Y. Kanno, K.Y. Inoue, A. Suda, R. Kunikata, M. Matsudaira,
587 Y. Takahashi, H. Shiku, T. Matsue, *Anal. Chem.* **2015**, *87*, 6364-6370.
588 [72] Y. Kanno, K. Ino, H. Abe, C. Sakamoto, T. Onodera, K.Y. Inoue, A. Suda, R.
589 Kunikata, M. Matsudaira, H. Shiku, T. Matsue, *Anal. Chem.* **2017**, *89*, 12778-12786.
590 [73] K. Ino, T. Onodera, Y. Kanno, A. Suda, R. Kunikata, T. Matsue, H. Shiku,
591 *Electrochim. Acta* **2018**, *268*, 554-561.
592 [74] C. Thery, L. Zitvogel, S. Amigorena, *Nat. Rev. Immunol.* **2002**, *2*, 569-579.
593 [75] S. Wang, L. Zhang, S. Wan, S. Cansiz, C. Cui, Y. Liu, R. Cai, C. Hong, I.T. Teng, M.
594 Shi, Y. Wu, Y. Dong, W. Tan, *ACS Nano* **2017**, *11*, 3943-3949.
595 [76] J. Zhang, L.L. Wang, M.F. Hou, Y.K. Xia, W.H. He, A. Yan, Y.P. Weng, L.P. Zeng, J.H.
596 Chen, *Biosens. Bioelectron.* **2018**, *102*, 33-40.
597 [77] Y. Nashimoto, Y. Takahashi, H. Ida, Y. Matsumae, K. Ino, H. Shiku, T. Matsue, *Anal.*
598 *Chem.* **2015**, *87*, 2542-2545.
599 [78] H. Ida, Y. Takahashi, A. Kumatani, H. Shiku, T. Matsue, *Anal. Chem.* **2017**, *89*,
600 6015-6020.
601 [79] Y. Takahashi, A. Kumatani, H. Shiku, T. Matsue, *Anal. Chem.* **2017**, *89*, 342-357.
602 [80] M. Sen, Y. Takahashi, Y. Matsumae, Y. Horiguchi, A. Kumatani, K. Ino, H. Shiku, T.
603 Matsue, *Anal. Chem.* **2015**, *87*, 3484-3489.
604 [81] Y. Takahashi, H. Ida, Y. Matsumae, H. Komaki, Y. Zhou, A. Kumatani, M. Kanzaki,
605 H. Shiku, T. Matsue, *Phys. Chem. Chem. Phys.* **2017**, *19*, 26728-26733.
606 [82] K. Ino, Y. Kanno, T. Nishijo, T. Goto, T. Arai, Y. Takahashi, H. Shiku, T. Matsue,
607 *Chem. Commun.* **2012**, *48*, 8505-8507.
608 [83] K. Ino, Y. Kanno, T. Nishijo, H. Komaki, Y. Yamada, S. Yoshida, Y. Takahashi, H.
609 Shiku, T. Matsue, *Anal. Chem.* **2014**, *86*, 4016-4023.
610 [84] K. Ino, T. Nishijo, T. Arai, Y. Kanno, Y. Takahashi, H. Shiku, T. Matsue, *Angew.*
611 *Chem. Int. Ed.* **2012**, *51*, 6648-6652.

[85] K. Ino, T. Nishijo, Y. Kanno, F. Ozawa, T. Arai, Y. Takahashi, H. Shiku, T. Matsue, *Electrochemistry* **2013**, *81*, 682-687.
[86] K. Ino, Y. Kitagawa, T. Watanabe, H. Shiku, M. Koide, T. Itayama, T. Yasukawa, T. Matsue, *Electrophoresis* **2009**, *30*, 3406-3412.
[87] Z. Lin, Y. Takahashi, T. Murata, M. Takeda, K. Ino, H. Shiku, T. Matsue, *Angew. Chem. Int. Ed.* **2009**, *48*, 2044-2046.
[88] M. Sen, K. Ino, H. Shiku, T. Matsue, *Biotechnol. Bioeng.* **2012**, *109*, 2163-2167.
[89] M. Takeda, H. Shiku, K. Ino, T. Matsue, *Analyst* **2011**, *136*, 4991-4996.
[90] T. Tschirhart, X.Y. Zhou, H. Ueda, C.Y. Tsao, E. Kim, G.F. Payne, W.E. Bentley, *ACS Synth. Biol.* **2016**, *5*, 28-35.
[91] J.J. Gooding, *Electroanalysis* **2002**, *14*, 1149-1156.
[92] J. Liu, H. Zhou, J.-J. Xu, H.-Y. Chen, *Analyst* **2012**, *137*, 3940-3945.
[93] R.A. Nascimento, R.E. Ozel, W.H. Mak, M. Mulato, B. Singaram, N. Pourmand, *Nano Lett.* **2016**, *16*, 1194-1200.
[94] M.H. Asif, S.M. Ali, O. Nur, M. Willander, C. Brannmark, P. Stralfors, U.H. Englund, F. Elinder, B. Danielsson, *Biosens. Bioelectron.* **2010**, *25*, 2205-2211.
[95] R. Pan, M. Xu, D. Jiang, J.D. Burgess, H.Y. Chen, *Proc. Natl. Acad. Sci. U. S. A.* **2016**, *113*, 11436-11440.
[96] R. He, H. Tang, D. Jiang, H.-y. Chen, *Anal. Chem.* **2016**, *88*, 2006-2009.
[97] H. Zhang, B. Li, Z. Sun, H. Zhou, S. Zhang, *Chem. Sci.* **2017**, *8*, 8025-8029.
[98] J. Xu, P. Huang, Y. Qin, D. Jiang, H.Y. Chen, *Anal. Chem.* **2016**, *88*, 4609-4612.
[99] J. Zhou, G. Ma, Y. Chen, D. Fang, D. Jiang, H.Y. Chen, *Anal. Chem.* **2015**, *87*, 8138-8143.
[100] H. Xu, S. Zhou, D. Jiang, H.Y. Chen, *Anal. Chem.* **2018**, *90*, 1054-1058.
[101] J. Xu, D. Jiang, Y. Qin, J. Xia, D. Jiang, H.Y. Chen, *Anal. Chem.* **2017**, *89*, 2216-2220.
[102] G. Liu, C. Ma, B.K. Jin, Z. Chen, J.J. Zhu, *Anal. Chem.* **2018**, *90*, 4801-4806.
[103] A.J. Bard, M. Stratmann, P.R. Unwin, Instrumentation and electroanalytical chemistry, Wiley-VCH2003.
[104] J. Ramon-Azcon, E. Valera, A. Rodriguez, A. Barranco, B. Alfaro, F. Sanchez-Baeza, M.P. Marco, *Biosens. Bioelectron.* **2008**, *23*, 1367-1373.
[105] L. Alfonta, A. Bardea, O. Khersonsky, E. Katz, I. Willner, *Biosens. Bioelectron.* **2001**, *16*, 675-687.
[106] C.J. Felice, M.E. Valentinuzzi, *IEEE Trans. Biomed. Eng.* **1999**, *46*, 1483-1487.
[107] J. Wegener, C.R. Keese, I. Giaever, *Exp. Cell Res.* **2000**, *259*, 158-166.
[108] J. Abbott, T. Ye, L. Qin, M. Jorgolli, R.S. Gertner, D. Ham, H. Park, *Nat.*

*Nanotechnol.* **2017**, *12*, 460-466.
[109] Q. Li, G.K. Tofaris, J.J. Davis, *Anal. Chem.* **2017**, *89*, 3184-3190.
[110] S.N. Bhatia, D.E. Ingber, *Nat. Biotechnol.* **2014**, *32*, 760-772.
[111] Y. Nashimoto, T. Hayashi, I. Kunita, A. Nakamasu, Y.S. Torisawa, M. Nakayama, H. Takigawa-Imamura, H. Kotera, K. Nishiyama, T. Miura, R. Yokokawa, *Integr. Biol.* **2017**, *9*, 506-518.
[112] C.X. Guo, S.R. Ng, S.Y. Khoo, X. Zheng, P. Chen, C.M. Li, *ACS Nano* **2012**, *6*, 6944-6951.
[113] S. Isik, M. Etienne, J. Oni, A. Blochl, S. Reiter, W. Schuhmann, *Anal. Chem.* **2004**, *76*, 6389-6394.
[114] E. Kim, W.T. Leverage, Y. Liu, I.M. White, W.E. Bentley, G.F. Payne, *Analyst* **2014**, *139*, 32-43.
[115] F. Ozawa, K. Ino, T. Arai, J. Ramon-Azcon, Y. Takahashi, H. Shiku, T. Matsue, *Lab Chip* **2013**, *13*, 3128-3135.
[116] F. Ozawa, K. Ino, H. Shiku, T. Matsue, *Materials* **2016**, *9*, 744.
[117] N. Taira, K. Ino, J. Robert, H. Shiku, *Electrochim. Acta* **2018**, *281*, 429-436.

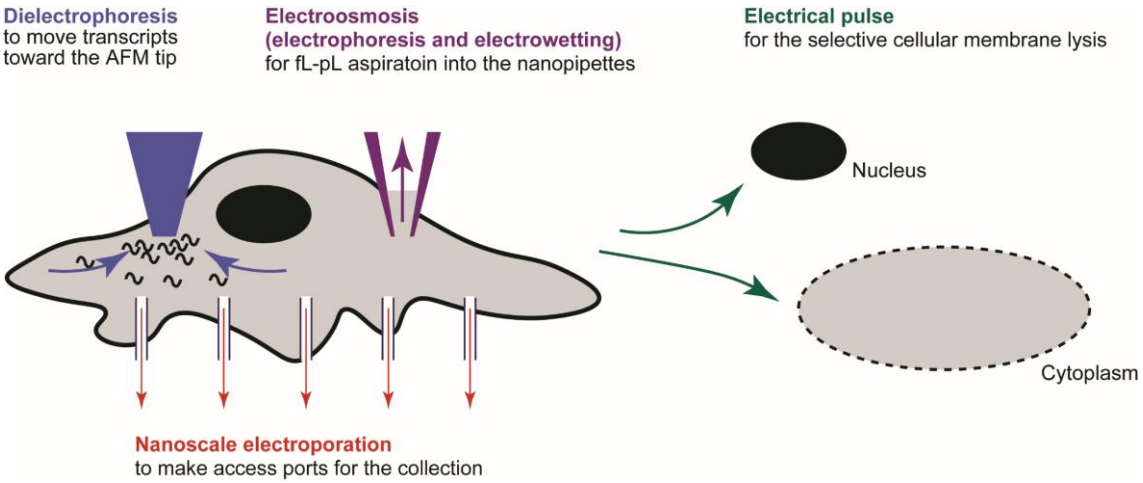


**Figure 1**

Overview of electrical techniques for the collection of subcellular cytoplasm utilizing dielectrophoresis, electroosmosis, electrophoresis, electrowetting, and electrical pulse.

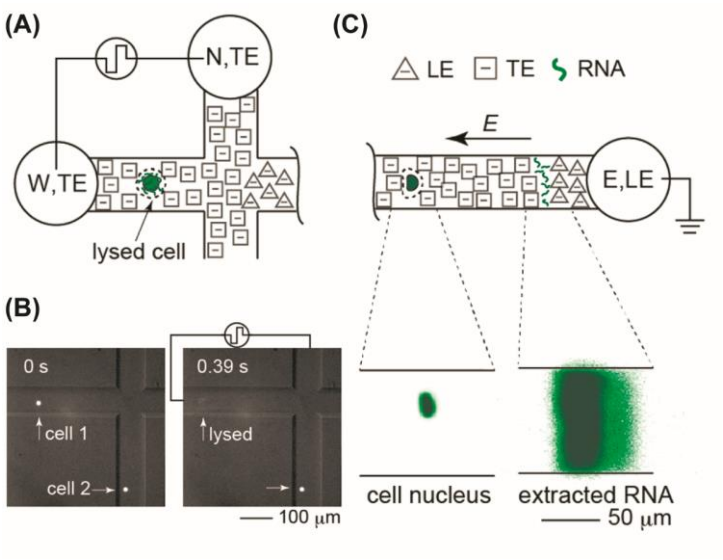


**Figure 2**

Selective electrical lysis of the cellular membrane, and analysis of the nucleus and cytoplasmic RNA using ITP. (A) Schematic of selective lysis of the cellular membrane. The electrical pulse is applied between the north (N) and west (W) reservoirs. (B) Representative micrographs of cellular membrane lysis. Only cell 1 is lysed. Cell 2 is intact because it did not enter the channel for cell lysis. (C) Typical images of the cell nucleus and extracted cytoplasmic RNAs fluorescently labeled with SYBR Green II. The color scales of the cell nucleus and cytoplasmic RNAs are different, for clarity. Adapted with permission from reference [26]. Copyright 2014 American Chemical Society.

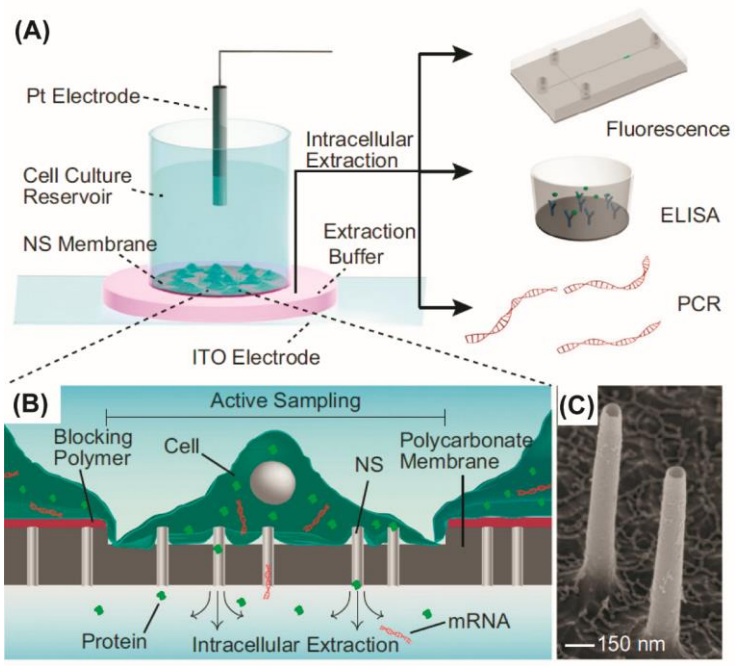


**Figure 3**

Nanostraw extraction (NEX). (A) Schematic of the NEX setup. Target cells are cultured on a polymer membrane with nanostraws. A Pt electrode is inserted into the cell culture reservoir and an ITO electrode is placed at the bottom of the extraction area. These electrodes are used for nanoelectroporation, generating openings in the cellular membrane at the nanostraw tips. (B) Enlarged schematic view of the membrane. Intracellular contents diffuse into the extraction buffer through the nanostraws. (C) Tilted scanning electronic microscopy (SEM) image of nanostraws with diameter of 150 nm. Adapted from reference [30].

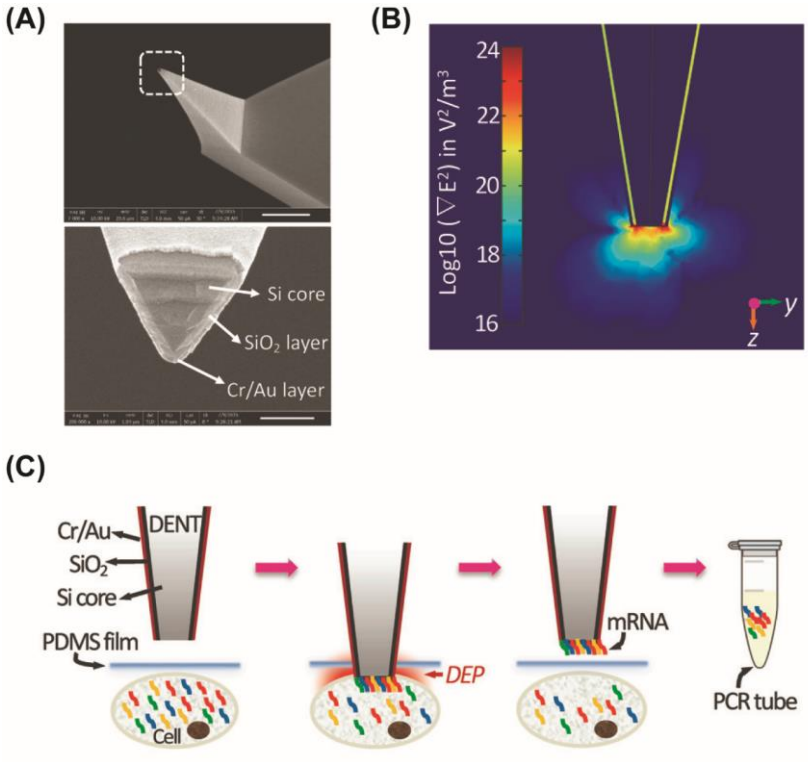


**Figure 4**

Dielectrophoretic nanotweezer (DENT). (A) SEM image of DENT. The lower image is an enlarged view of the white broken rectangle area in the upper image. Three layers (Si core, $SiO_2$, and Cr/Au) can be distinguished. (B) Simulation of the gradient in the electric field square when 1.5 V AC field is applied between the Si core and Cr/Au electrode in the cytoplasm. (C) Schematic of the process of mRNA collection using DENT. After the insertion of DENT into the cytoplasm, DRP force is generated at the DENT tip. The DEP force attracts mRNA from the cytoplasm. After the collection, DENT probe is withdrawn and the collected mRNA is analyzed by qPCR or RNA-seq. Adapted with permission from reference [40]. Copyright 2017 Royal Society of Chemistry.

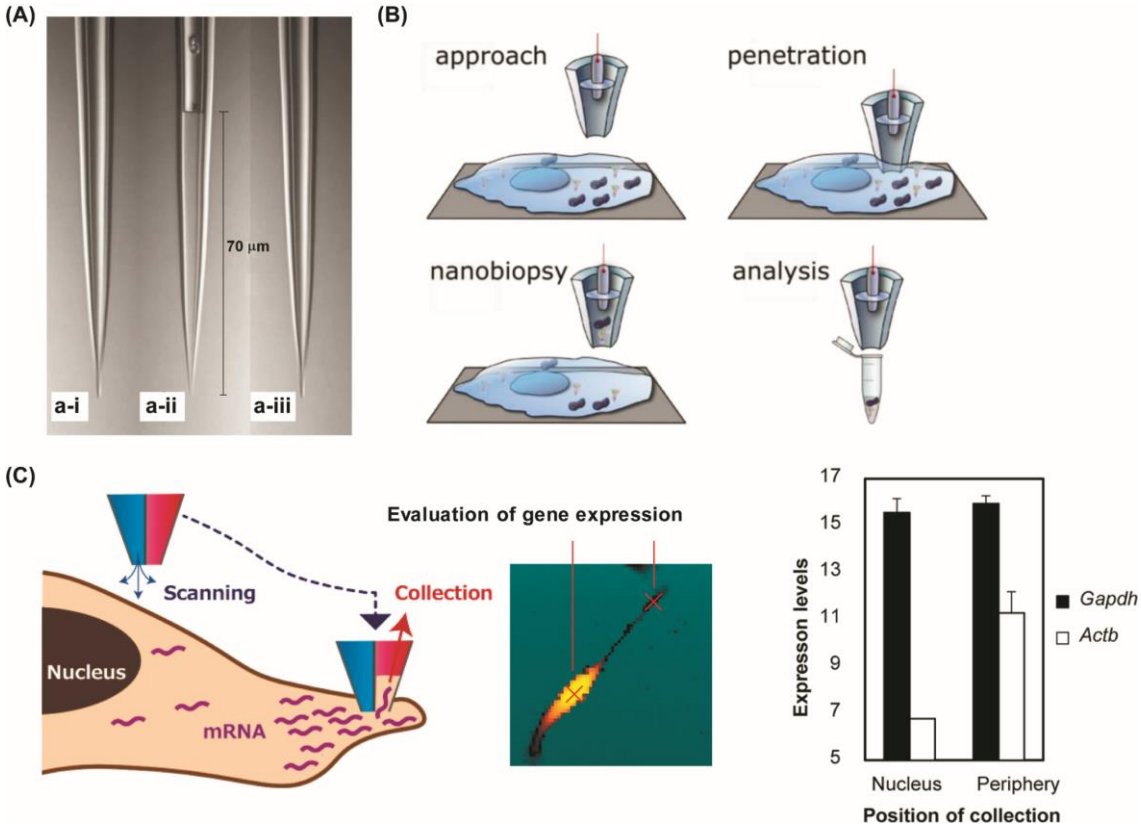


**Figure 5**

Integration of an electrochemical attosyringe with SICM. (A) Regulation of an oil-water interface by a potential applied to the electrode in the nanopipette (E). Images when when E is (a-i) +600 mV, (a-ii) –100 mV, and (a-iii) +600 mV. Adapted with permission from reference [58]. Copyright 2007 National Academy of Sciences. (B) Nanobiopsy sequence. Following the approach of the nanopipette based on the ion current at the tip, the pipette moves down and penetrates the cellular membrane. After the collection of the cytoplasm using the electrochemical attosyringe, the nanopipette moves up, and the cellular contents are analyzed by qPCR or next-generation sequencing. Adapted with permission from reference [59]. Copyright 2014 American Chemical Society. (C) High-resolution imaging using a nanobiopsy probe. (Left) Schematic of the collection process. A nanoscale image of the target single cell is first acquired using aqueous barrel. Then, the nanopipette moves to the collection position using the information from the nanoscale image (nanoscale map, center). (Right) qPCR data for gene expression in the cytoplasm near the nucleus and at the periphery of the same single cell. *Actb* expression levels are different depending on the cellular location, while the expression of *Gapdh* is nearly unchanged. Adapted with permission from reference [62]. Copyright 2016 American Chemical Society.

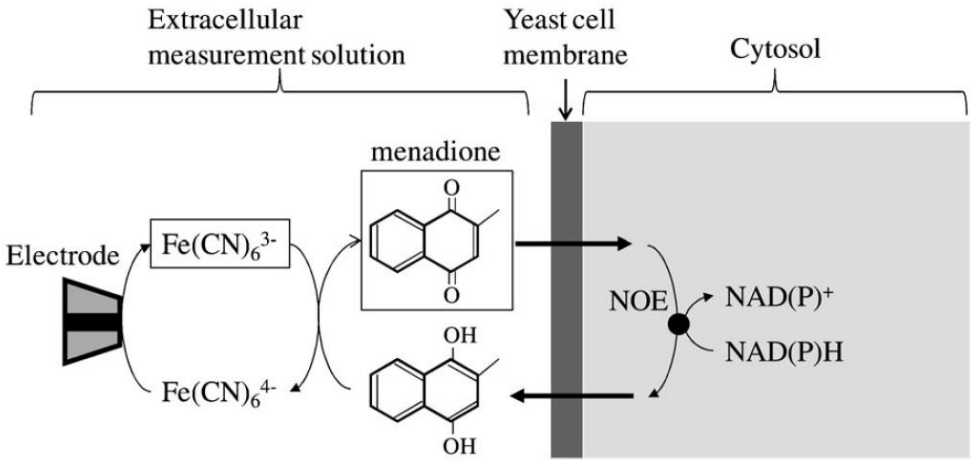


**Figure 6**

Double-mediator system for the detection of intracellular enzymes [64]. A system using menadione and $[Fe(CN)_6]^{3-}$ for NOE detection is shown. Reproduced with permission from WILEY-VCH Verlag GmbH & Co. ©2011.

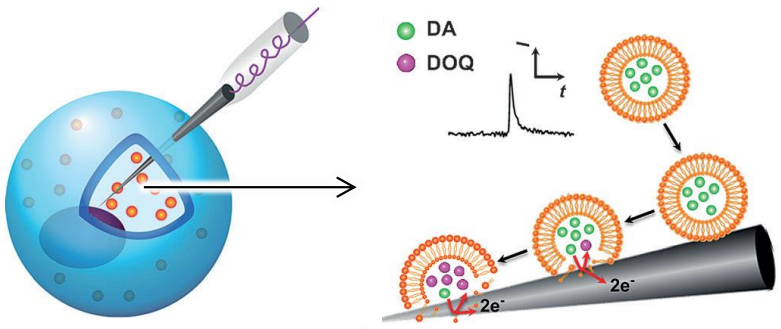


**Figure 7**

Detection of intracellular vesicles containing dopamine (DA) [70]. DA is oxidized to dopamine orthoquinone (DOQ) at the nanotip electrode. Reproduced with permission from Wiley-VCH Verlag GmbH &Co. ©2015.

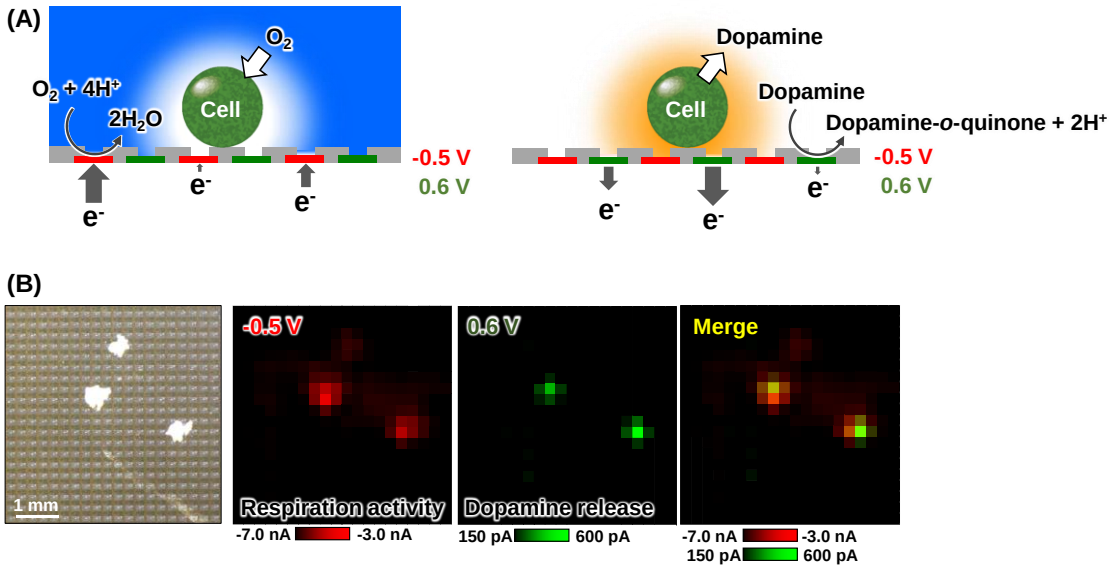


**Figure 8**

Electrochemicolor imaging of the respiratory activity and dopamine release from aggregates of neuron-like cells [72]. (A) Detection schemes. (B) Optical and electrochemical images of the aggregates. Electrochemical images at –0.5 and +0.6 V show respiratory activity and dopamine release, respectively. Reproduced with permission from the American Chemical Society ©2017.

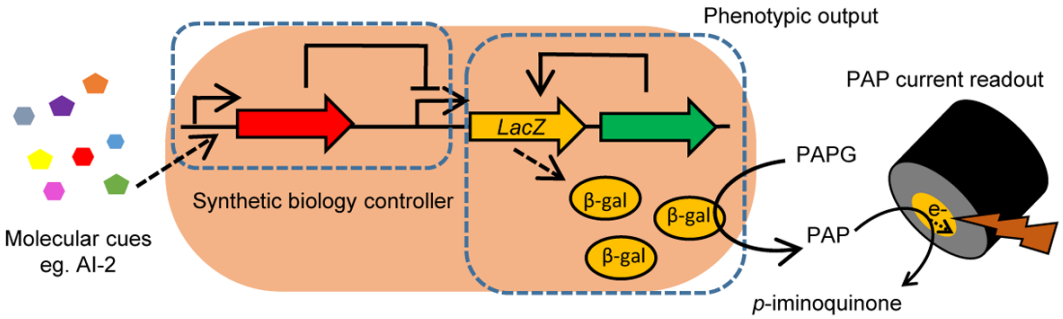


**Figure 9**

Electrochemical reporter gene assay. In this example, *β*-galactosidase (*β*-gal) is used as a reporter, and the expression of its gene is induced by various molecular cues [90]. PAPG, the enzymatic substrate, is converted by *β*-gal to PAP. PAP levels are then quantified using an electrode set outside the cells. Reproduced with permission from the American Chemical Society ©2015.

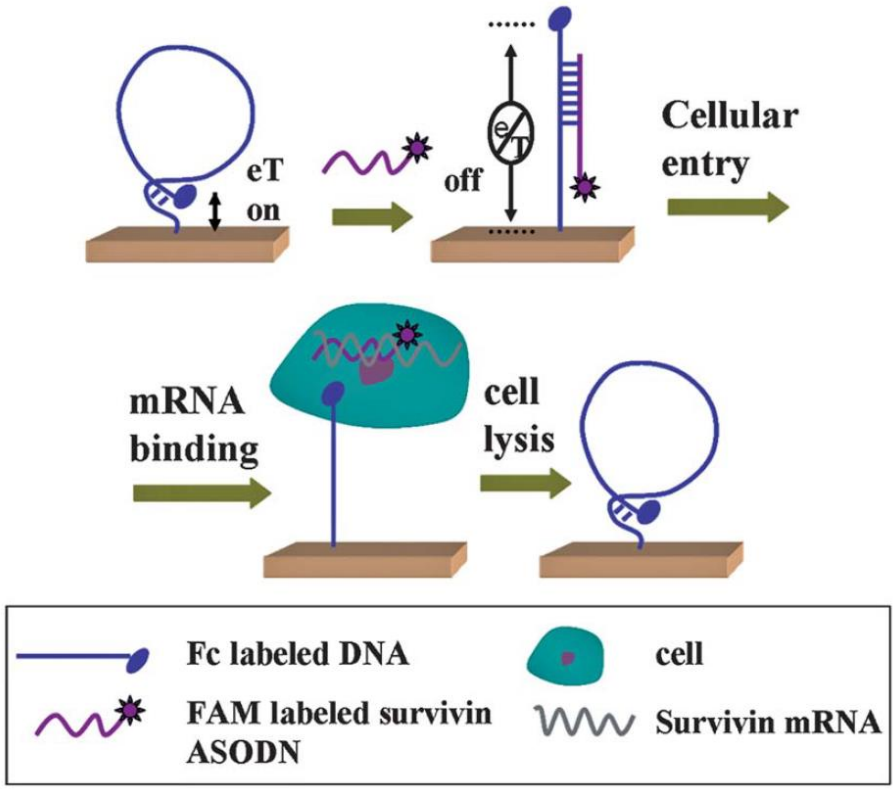


**Figure 10**

Fc-DNA–based electrochemical sensor for mRNA in living cells [92]. The redox signal at the sensor is altered in the presence of *survivin* mRNA. Reproduced with permission from the Royal Society of Chemistry ©2012.

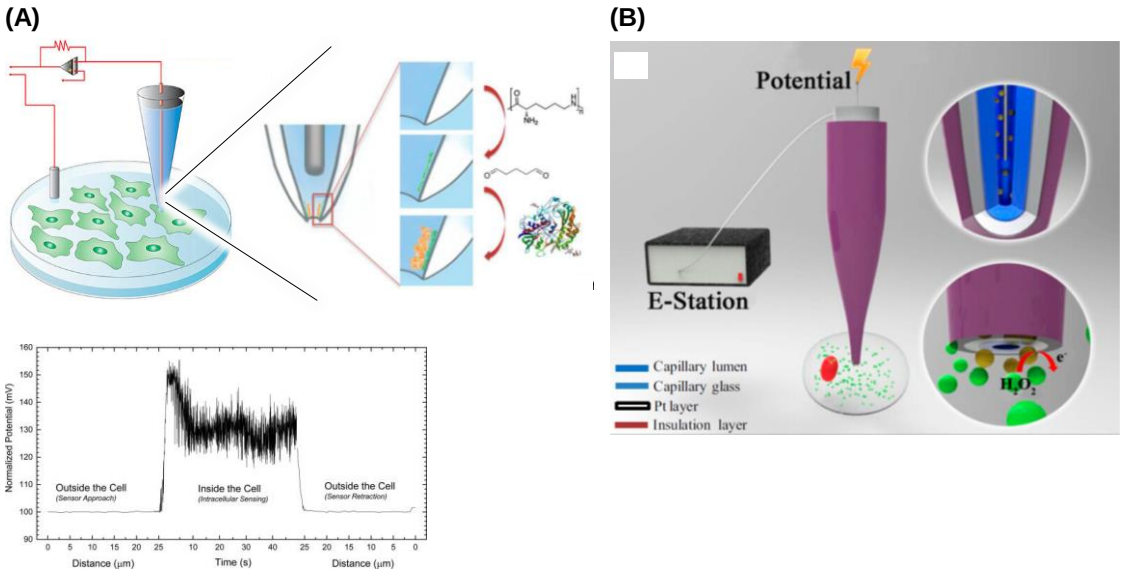


**Figure 11**

Intracellular glucose sensing. (A) Potentiometric sensing using a nanopipette [93]. GOx is immobilized on the surface inside the nanopipette. Glucose is oxidized to gluconic acid by GOx, resulting in a change of impedance. (B) Nanometer-sized capillary with a ring electrode for glucose detection within cells [85]. A kit is introduced into the cells through the capillary, and glucose is detected based on $H_2O_2$ production. Reproduced with permission from the American Chemical Society ©2016, and the National Academy of Sciences ©2016, respectively.

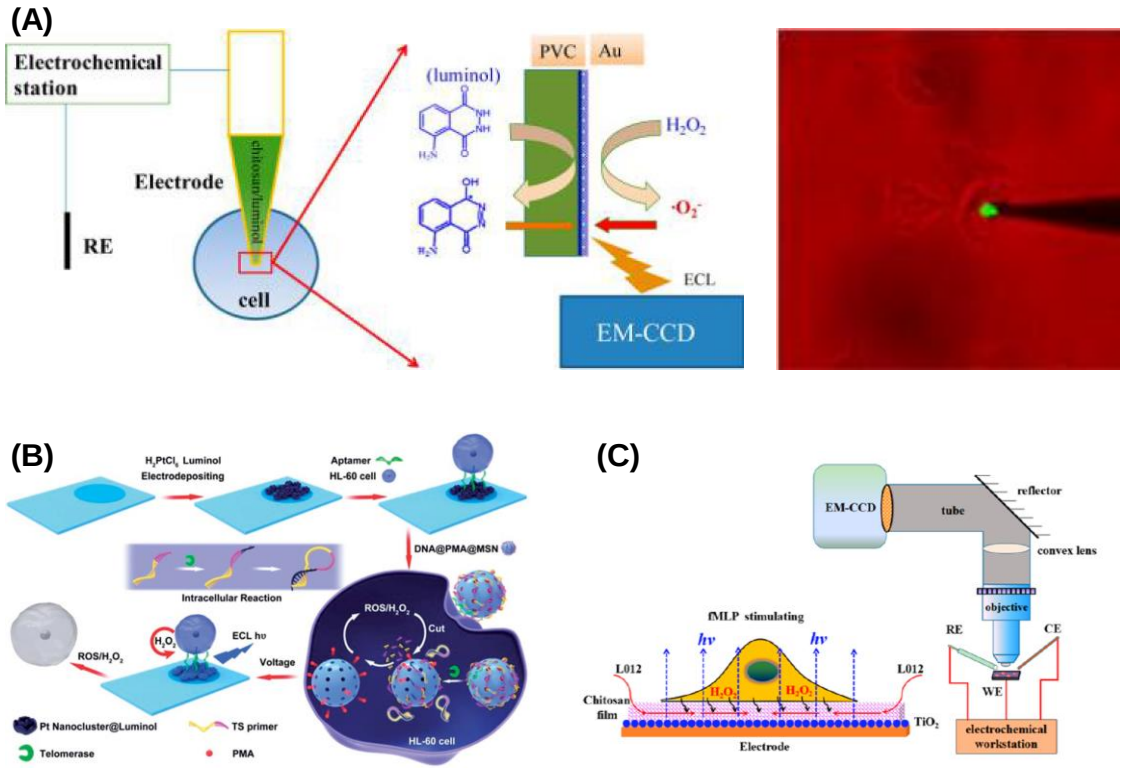


**Figure 12**

ECL for intracellular sensing. (A) Detection of intracellular $H_2O_2$ [96]. (B) Detection of intracellular telomerase [97]. (C) ECL imaging of cells using chitosan and fluoride-doped tin oxide conductive glass modified using nano-$TiO_2$ [102]. Reproduced with permission from the American Chemical Society ©2016 (A) and 2018 (B), and the Royal Society of Chemistry ©2017 (C).